

Volumetric Lagrangian Particle Velocity and Temperature Measurements in large aspect ratio Rayleigh-Bénard Convection

T. Käufer^{1,*}, C. Cierpka¹

1: Institute for Thermodynamics and Fluid Mechanics, Technische Universität Ilmenau, Germany

*Corresponding author: theo.kaeufer@tu-ilmenau.de

Keywords: Temperature measurements, PIT, Velocity measurements, STB, Color imaging, Heat transfer, Rayleigh-Bénard convection

ABSTRACT

Rayleigh-Bénard convection (RBC) is a well-known model experiment for temperature-driven flows. Even though RBC has been studied for decades, many open questions remain. Temporally and spatially resolved temperature and velocity data are crucial for a better understanding of the underlying physics. This paper proposes a new approach that combines Lagrangian Particle Tracking (LPT) with Particle Image Thermometry (PIT). The combined measurement techniques should be utilized to investigate the flow inside a large aspect ratio RBC cell with a lateral size of

$w = 700$ mm and a height $h = 28$ mm, which corresponds to an aspect ratio $\Gamma = \frac{w}{h} = 25$. Due to the large aspect ratio, the cameras observe the flow through the transparent cooling plate. We show that LPT of thermal convection flows within the setup can be performed successfully. Subsequently, we describe the temperature measurement technique PIT based on Thermochromic Liquid Crystals (TLCs) and discuss and quantify the additional challenge arising from color imaging of small particles. Namely, the sparse color sampling of a color filter array (CFA) camera and chromatic dispersion resulting from the oblique viewing angle of the color camera. To circumvent the sparse sampling of the CFA camera, we use a three-chip camera that resolves each color (red, green, blue) at full sensor resolution. We quantify the influence of the chromatic dispersion by cross-correlating the color channels. We then apply the resulting disparity maps in a correcting step to reduce the disparities by shifting the red and blue towards the green channel. The visual comparison of the corrected and uncorrected images shows a reduction in the color dispersion. Beyond that, the remaining disparities between the colors of the corrected images are minimal. This indicates that the correction step is useful to increase the quality of the particle images for temperature estimation.

1. Introduction

In many cases, fluid flows are connected with heat transfer. One prominent example is the Rayleigh-Bénard convection (RBC) which is a simple model of thermally-driven flow that is widely studied, e.g., see (Chillà & Schumacher, 2012) and (Castaing et al., 1989). An RBC experiment typically consists of a fluid confined by a heating plate at the top, a cooling plate at the bottom, and adiabatic sidewalls. Even though RBC has been extensively studied, the phenomena are not yet fully

understood. One such example is the formation of large-scale structures in turbulent RBC of large aspect ratio (Pandey et al., 2018). The aspect ratio Γ is the ratio between the convection cell's lateral size w and height h .

Numerical long-time studies of those flow structures are extremely computationally costly and are currently a limiting factor in their investigation. Therefore, combined stereoscopic Particle Image Velocimetry (PIV) and Particle Image Thermometry (PIT) using encapsulated Thermochromic Liquid Crystals (TLCs) as seeding particles were successfully performed in the past by Moller et al. (2021). PIT is a temperature measurement technique that utilizes the property of the TLCs to reflect light of different color depending on their temperature when illuminated with white light. A color camera then captures the reflected colored particle images. Additionally, the TLC particles can be used as conventional tracer particles for PIV or Particle Tracking Velocimetry (PTV).

The next step is to extend the measurement technique to fully volumetric velocity and temperature measurements. Different approaches in this direction have been made in the past. Segura et al. (2015) combined Astigmatism Particle Tracking Velocimetry (APTV) and PIT for combined 3D velocity and temperature measurements inside a droplet. The authors utilized non-encapsulated TLC particles as seeding and a 3-chip-camera to capture the reflected light. The authors have shown that the combined approach is promising and report an uncertainty of 0.1 K for the temperature measurements over a range of 1.5 K and an uncertainty in the depth estimation of 1.7 for a depth range of 20 μm . However, the measurements were performed on micro-scale, where the extraction of reliable color values is simpler due to the much larger particle images. Therefore the measurement technique can not be directly transferred for macroscopic applications.

Schiepel et al. (2021) combined tomographic PIV and PIT to measure both the velocity and the temperature in a volume inside an aspect ratio $\Gamma = 1$ RBC cell. The authors used four monochrome cameras for the tomographic PIV measurement and an additional color camera to capture the particle color. They have successfully demonstrated that PIT can be used for volumetric measurements on a macroscopic scale and report a temperature uncertainty of 0.095 K for a temperature range of 2 K. One drawback of the proposed method is the computational overhead by combining tomographic PIV, which generates velocity vectors on a regular grid with PIT, which estimates the particle temperature at its position. Furthermore, the authors used very large TLC particles which require a laborious density adjustment of the fluid.

In this paper, we propose a method that leverages the benefits of Lagrangian Particle Tracking (LPT) and uses the obtained information about the particle position to estimate the particle temperature by evaluating the color of the particle image. Additionally, we aim to use smaller particles with a size below 40 μm , which are much more common and do not require a density matching procedure between particles and fluid. We also discuss the challenges that arise from color imaging of small particles, like the sparse spatial color sampling of a color filter array (CFA) camera and chromatic dispersion.

2. Experimental setup

The measurement technique should be applied to measure the fluid properties in large aspect ratio RBC. The experimental setup is shown in Figure 1. The central part of the experiment is a RBC

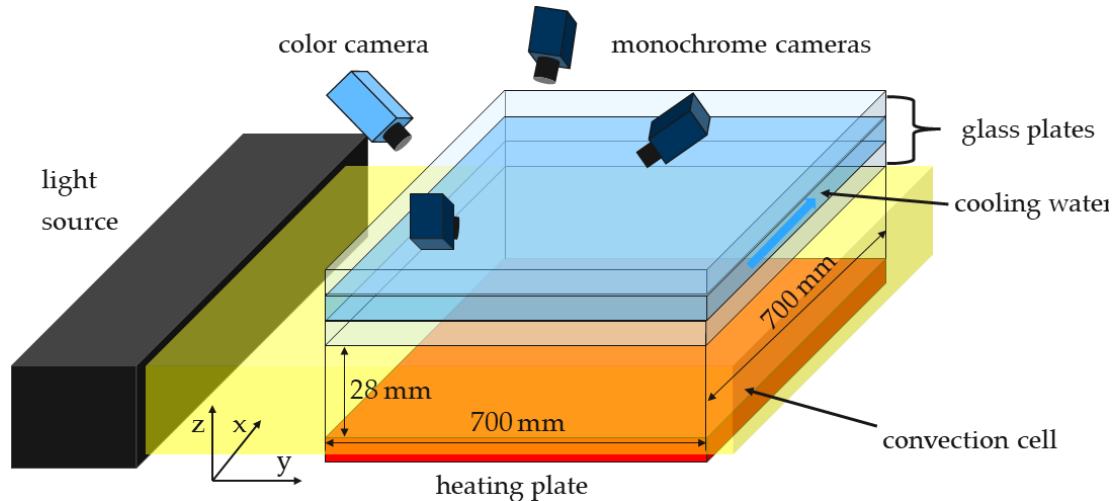


Figure 1. Sketch of the experiment and the measurement arrangement.

cell with a lateral size $w = 700$ mm and a height $h = 28$ mm which corresponds to an aspect ratio $\Gamma = \frac{w}{h} = 25$. The heating plate at the bottom is made from aluminum and heated by water flowing through it. The side walls are made out of glass such that the inside of the cell can be illuminated. The cooling plate at the top consists of two glass plates that are slightly separated. Between those plates cooling water can pass through to cool the experiment from the top. The cooling plate assembly provides the optical access from above, which is necessary in order to achieve a reasonable measurement area in a large aspect ratio RBC cell as explained by Cierpka et al. (2019). Both the temperature in the cooling plate as well as in the heating plate is adjusted by thermostats and monitored by Pt-100 temperature sensors which have an individual uncertainty of 0.1 K. To visualize the flow, polymer-encapsulated TLC seeding particles of type R20C20W and R25C50W (LCR Hallcrest) with a nominal starting temperature of 20 °C and temperature range of 20 °C and 25 °C and 50 °C, respectively, are being used. The particles are illuminated by a custom-made white light LED array shown at the left of Fig. 1. The LED array has a broad illumination spectrum ranging from ≈ 430 nm to ≈ 700 nm. The TLC seeding particles are imaged by a three monochrome (sCMOS PCO edge 5.5, LaVision GmbH / Excelitas PCO GmbH) and one color camera. The color camera is either a color filter array (CFA) camera (sCMOS PCO edge 5.5 color, Excelitas PCO GmbH) or a three-chip camera (3-CMOS JAI Apex AP-3200T-USB, JAI Ltd.). The joint field of view (FOV) of all cameras is about 160 mm \times 160 mm.

3. Measurement techniques

The main principle of the combined temperature measurement approach is to combine Lagrangian velocity and positional data obtained through the commercially available version of Shake-the-Box (LaVision GmbH) with a custom-made Particle Image Thermometry processing. After the separate velocity and temperature processing, the results of both measurements can be combined. Thereby it will be possible to access temperature and velocity at the same point in space and time, and if the data is needed on an Eulerian grid Radial Basis Function regression can be used for interpolation (Ratz et al., 2022). Figure 2 shows a graph of the processing scheme.

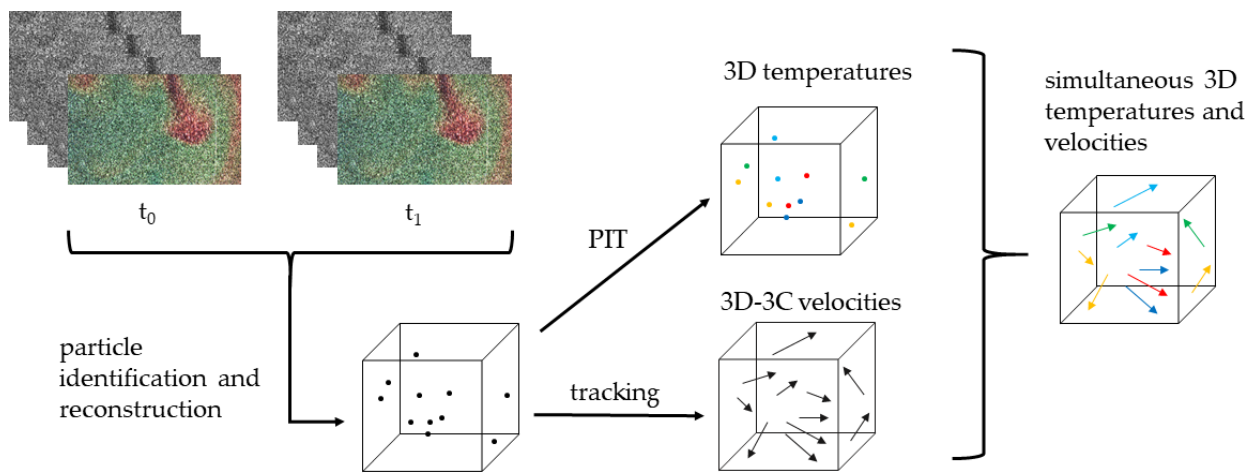


Figure 2. Scheme of the measurement principle

3.1. Velocity measurements

To calibrate the cameras, a dual-plane calibration target (Typ 204-15, LaVision GmbH) was positioned inside the RBC cell and images were recorded. Due to the small height of the cell, a dual plan calibration with an additional volumetric self-calibration using the particle images yielded the necessary calibration accuracy.

Figure 3 shows the particle positions obtained from 100 time steps of a STB measurement of thermal convection. The time between the frames amounts to 200 ms. Only particle positions that belong to tracks with a minimum length of 16 time steps are shown. The color displays the vertical velocity u_z . A red color indicates positive values of u_z and a blue color negative values of u_z . The plot in Figure 3 (a) shows the particle distribution in the measurement domain and region of distinct positive and negative u_z can be spotted. Additionally, Figure 3 (b) shows the projection of the particle positions into the x - y -plane. This projection clearly shows the typical cellular convection pattern, which can be seen as an indicator that volumetric Lagrangian velocity measurements using TLCs as tracer particles and LED illumination are feasible.

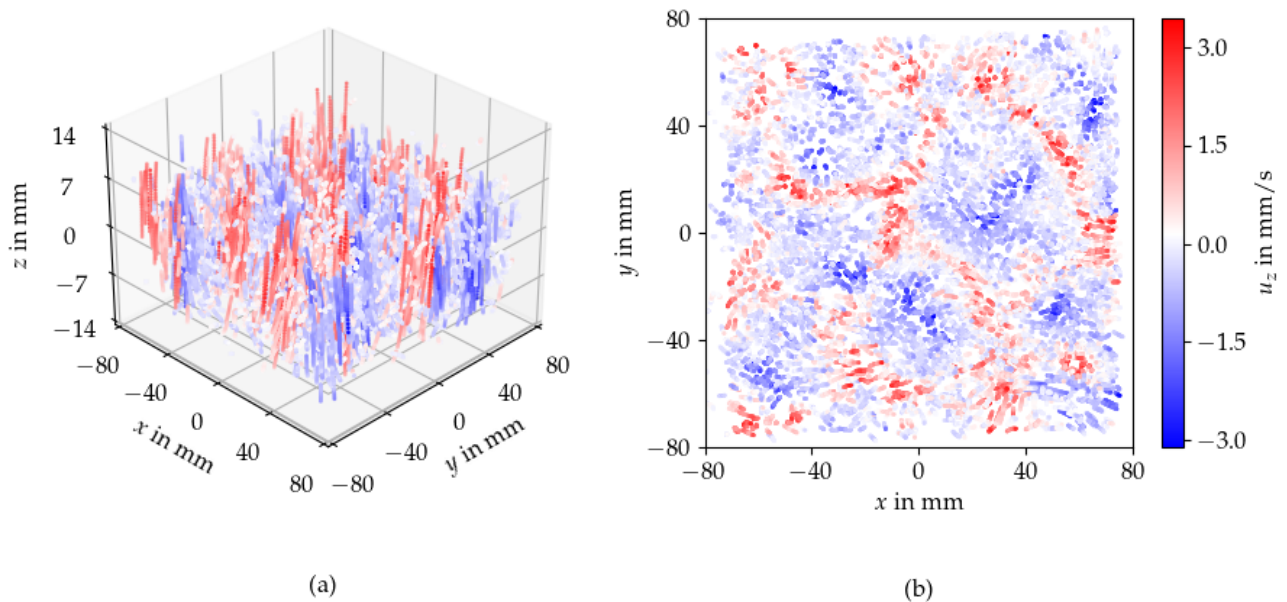


Figure 3. Isometric view (a) on the particle positions determined by STB measurements from 100 time steps of thermal convection. For this measurement, the three monochrome cameras and the CFA camera were used. Only particles that are a part of a trajectory with at length of at least 16 times steps are shown. The orientation of the coordinate system is the same as in Figure 1. The colors indicate the vertical velocity u_z . Red denotes positive and blue negative values. The projection of the particle position into the x - y -plane (b) clearly shows the convection pattern.

3.2. Temperature measurements

Quantitative temperature measurements with TLCs require a calibration since the mapping between color and temperature is not unique but affected by several factors. For example, the illumination spectrum and the angle θ between the illumination and the camera influence the initial temperature and the possible measurement range of the TLCs. At observation angles $\theta = 70^\circ - 80^\circ$, as used in the setup, the temperature range is significantly reduced, and the initial temperature is shifted to lower values compared to the nominal values. At the same time, the reduced measurement range leads to increased sensitivity since the same color change occurs in a much narrower temperature range. A detailed description of the influences is provided by Moller et al. (2019). For the calibration measurement, isothermal conditions are adjusted inside the whole convection cell. The temperature is then measured by the temperature sensors, and the color response of the TLCs is captured by the respective color camera. This step is then repeated for several temperatures across the desired measurement range. The correspondence between temperature can then be used to estimate the functional relations between those quantities, e.g., by local calibration functions of the hue value (Moller et al., 2019), neural networks (Anders et al., 2020; Moller et al., 2020), or a system matrix (Segura et al., 2013). After the calibration, the temperature can be derived from the color of the particle image.

While the determination of the particle colors in planar measurements can be achieved, e.g., by

spatial averaging over subdomains or interrogation windows analog to the segmentation performed for PIV measurement, the color determination for volumetric measurements is more complex since this approach would result in an averaging along the line of sight of the color camera. Hence, the color of each particle image has to be accessed individually during the actual flow measurements. Therefore, the 3D particle positions obtained by the STB are projected back into the image of the color camera (Fuchs et al., 2016), to detect the individual particle images. Even though this approach sounds straightforward, color imaging of very small particles comes with additional challenges compared to monochromatic images.

4. Color imaging of small particles

The color imaging of small particles that are illuminated by polychromatic light differs from the typical monochromatic imaging with monochromatic illumination. The most important factors that we want to discuss are the different recording principles of color cameras (Sec. 4.1) and the chromatic dispersion (Sec 4.2).

4.1. Recording of color images

In general, the pixels, which are the light-sensitive elements on the camera sensor, do not distinguish the different wavelengths they are exposed to. Hence, the different spectral components of the light need to be separated before the light incides on the sensor. The most common approach is a color filter array that is mounted onto the sensor. Thereby, pixels are only sensitive to a specific wavelength band corresponding to the specific filter. An example of a CFA called Bayer pattern is shown in Figure 4 (a). Thus the actual resolution of the image is reduced to one-half for the green and one-quarter for the red and blue color channel for the example of a Bayer pattern.

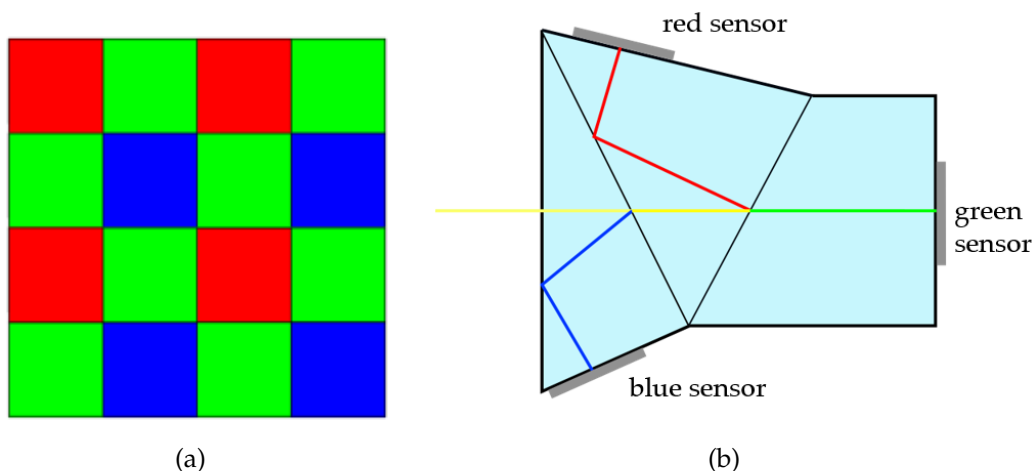


Figure 4. Two approaches to separate the spectral components of light for color imaging. A Bayer pattern (a) is used in the CFA color camera, and a trichroic prism (b) is used for color separation in the three-chip cameras.

Furthermore, an interpolation algorithm is required to reconstruct the actual color image at full resolution. A simple algorithm is the linear interpolation; however, many different and more advanced algorithms have been developed that, e.g., incorporate the morphology of the image. Gunturk et al. (2005) provide an overview of this topic. While this approach is relatively simple and often works well for photography and for many applications, the sparse resolution of the colors and the artifact resulting from the interpolation can negatively affect the correct color determination in cases where the particle image is approximately the size of the pixel. In such cases, a particle that appears blue but whose particle image is mostly projected onto a pixel behind a red filter would be registered as mostly red and therefore alter the correct color image.

One way to circumvent this is the use of a 3-chip prism camera that uses a trichroic prism and three sensors, one for each color channel, to record each color channel at full resolution, as shown in Figure 4 (b). Another advantage is that due to the reflective filters, the light is more effectively used compared to the absorptive filters used in a CFA camera. One important point to mention, however, is that each color is recorded on a different sensor. Therefore, it is important that the sensors are mechanically aligned with very high precision. Nevertheless, Hijazi et al. (2017) report a disparity between the color channels that we also observe. The disparities between the green and red (G-R) and between the green and blue (G-B) channels are shown in Figure 5. To compute the

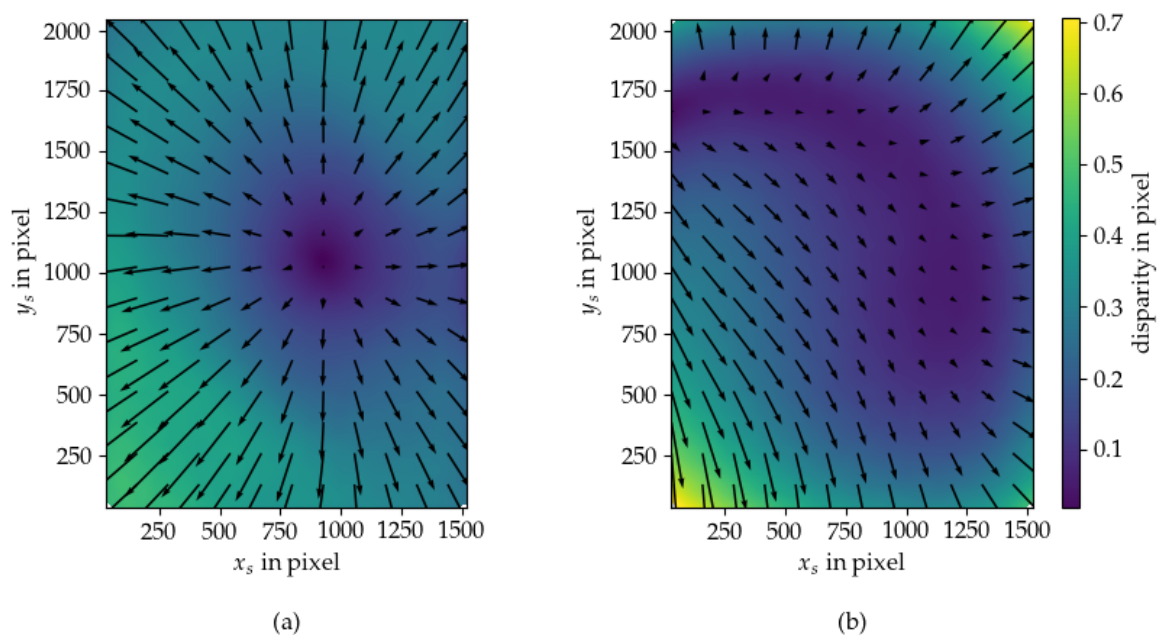


Figure 5. Disparity map between the green and red color channel (G-R) (a) and between green and blue color channel (G-B) (b) of the three-chip camera. The disparity map was computed from a printed particle pattern without change of the index of refraction in the optical path except for the camera optics.

disparity map, we recorded images of a printed particle pattern and then performed a PIV processing (sum-of-correlation over 100 image pairs, three passes, 64×64 window size with 75% overlap) between the green and red and between the green and blue channel. x_s and y_s are the projection of the x and y -axis shown in Figure 2 on to the camera sensor plane. The disparity maps show that the disparity G-R is small in the center of the image and increase towards the corners with a

maximum of 0.5 pixel at the bottom left. The shape of the disparity map indicates that the green and red sensor are well-aligned and that the disparity is mostly caused by a slight magnification shift between red and green sensor, as was reported by Hijazi et al. (2017). The disparity map G-B however, does not show a minimum at the image center but an irregular shape and a maximum disparity of 0.7 pixel at the bottom left. This might indicate that the green and blue sensors are slightly tilted. Nevertheless, the disparity of 0.7 pixel is very low, especially when considering that the pixel size of the camera is $3.45 \mu\text{m}$.

4.2. Chromatic dispersion

Another factor that negatively affects the color imaging of the small particles is chromatic dispersion. Chromatic dispersion is caused by the wavelength dependence of the index of refraction. When light is traveling through different media, the light is bent at the interfaces differently depending on its wavelength, and the light is dispersed into its spectral component, as qualitatively shown in Figure 6. The measurement setup presented in this paper is affected by this dispersion

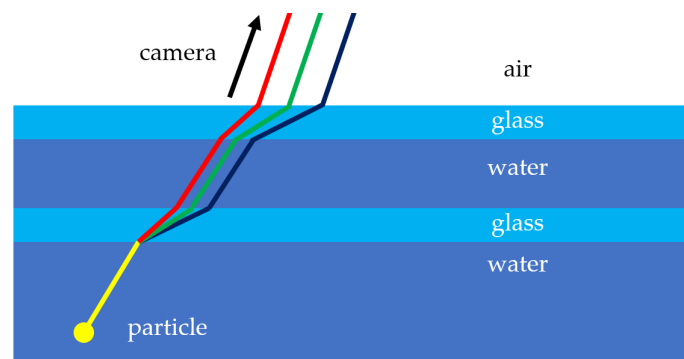


Figure 6. A principal sketch that qualitatively shows the effect of the chromatic dispersion caused by the cooling plate assembly.

since the color cameras are positioned obliquely with respect to the cooling plate assembly of the experiment. This is necessary to achieve a sufficient temperature measurement range. The effect of this color dispersion on the particle image can be seen in the picture (a) of Figure 7 and of Figure 8. The pictures show particle images recorded by the CFA camera (Fig. 7) and the three-chip camera (Fig. 8), respectively. The images were recorded under a central observation angle $\theta = 70^\circ$ for the CFA camera and $\theta = 80^\circ$ for the three-chip camera. Even though the images show different particles, the most obvious difference is the significantly differing particle image size which is primarily a result of the demosaicing processing of the CFA camera image that acts like a blurring filter and artificially increases the size of the particle images. Furthermore, by carefully looking at the pictures, one can distinguish the chromatic dispersion on the image of the individual particles. The particles appear slightly more red at the bottom, greener in the middle and blue at the upper particle image edge, especially in the CFA camera image. This makes the estimation of reliable color values particularly difficult.

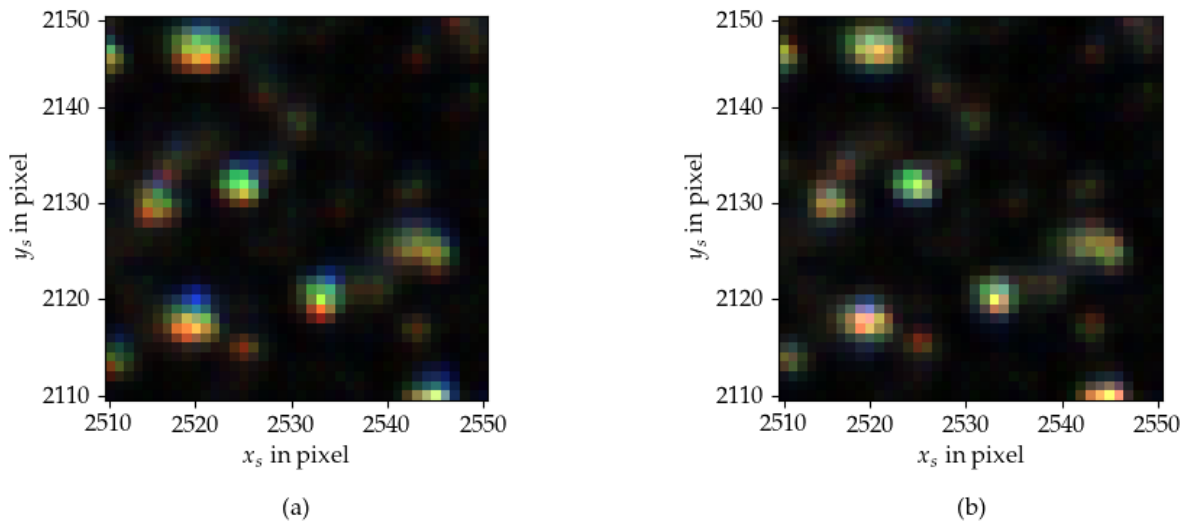


Figure 7. Particle image recorded by the CFA camera with sever chromatic dispersion (left) and the same particle image after the correction was applied (right). By comparing both images one can see that the color dispersion was significantly reduced.

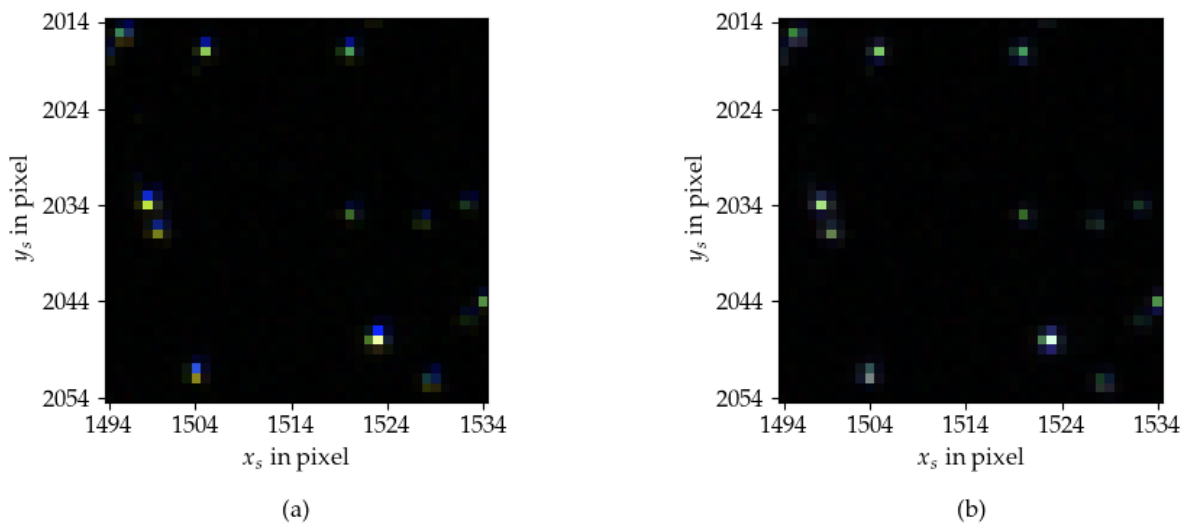


Figure 8. Particle image recorded by the three-chip camera with chromatic dispersion (a) and the same particle image after the correction was applied (b). By comparing both images, one can see that the color dispersion was significantly reduced.

To quantify the severity of the chromatic dispersion, the same approach and processing parameters as presented in Section 4 were applied to particle images of particles dissolved inside the experiment. The green and the red color channel and the green and blue color channel were cross-correlated. The results for the CFA camera are shown in Figure 9. Due to the opening angle of

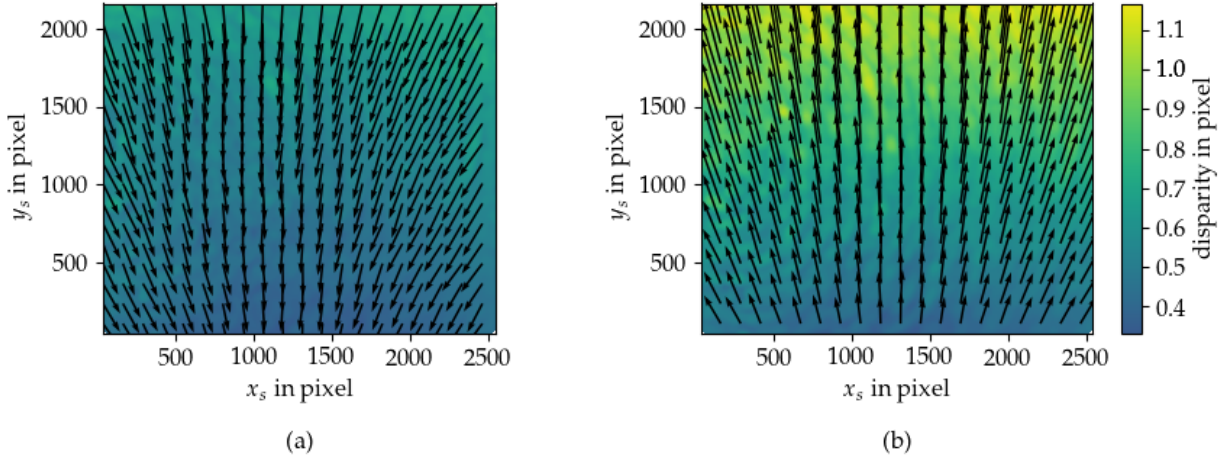


Figure 9. Disparity maps G-R (a) and G-B (b) of the CFA camera computed from particle images. The particle images were recorded with the cooling plate assembly in the optical path.

the camera, the observation angle decreases along the y_s -axis. This change can be clearly seen in the disparity maps. Resulting in higher disparities for lower observation angles, which is expected since, for lower observation angles, the light incident on the sensor is refracted more by the cooling plate assembly amplifying the chromatic dispersion. By comparing the absolute disparity values of G-R (Fig. 9(a)) and G-B (Fig. 9(b)). It can be seen that the disparities for G-R are about half the magnitude as for G-B.

Analogously, we applied the same processing to the images recorded by the three-chip camera. The images were recorded in a different experimental run. The resulting disparity maps are shown in Figure 10. Likewise, the disparity magnitude of G-R is lower than the disparity magnitude of G-B. However, the actual shape of the disparity maps of the CFA and three-chip camera differ. This is mostly related to the difference in the observation angle θ of the cameras and the superposition of the disparity related to the magnification difference and sensor misalignment of the three-chip camera and the disparity caused by the oblique viewing angle. A comprehensive view of the disparities is shown in Figure 11. The Figure shows the profile of the disparity component in y_s -direction, averaged along x_s , and plotted over y_s for G-R (red) and G-B (blue) for both color cameras. The profiles of the CFA camera (dashed lines) show the expected trend of an increasing disparity magnitude for increasing y_s values which is equivalent to a decreasing θ . The same trend can be observed for the disparity G-B of the three-chip camera (solid line), even though to a lesser extent which due to the larger central observation angle of the camera. The profile of G-R of the three-chip camera shows an inverse trend of the disparity.

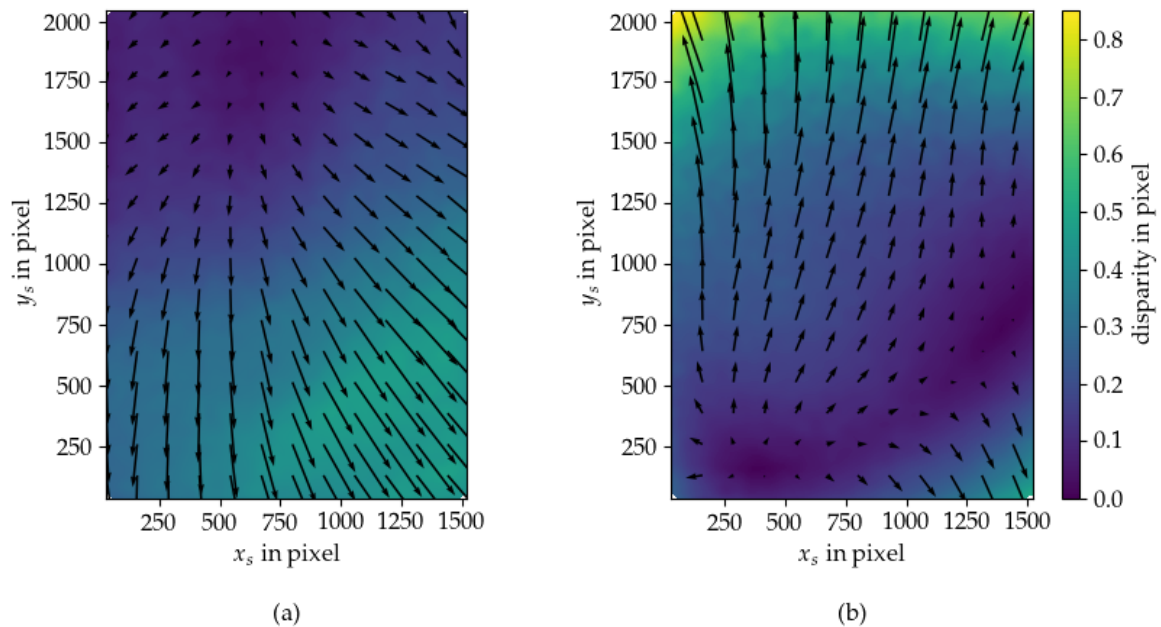


Figure 10. Disparity maps G-R (a) and G-B (b) of the three-chip camera in measurement configuration. The particle images were recorded with the cooling plate assembly in the optical path.

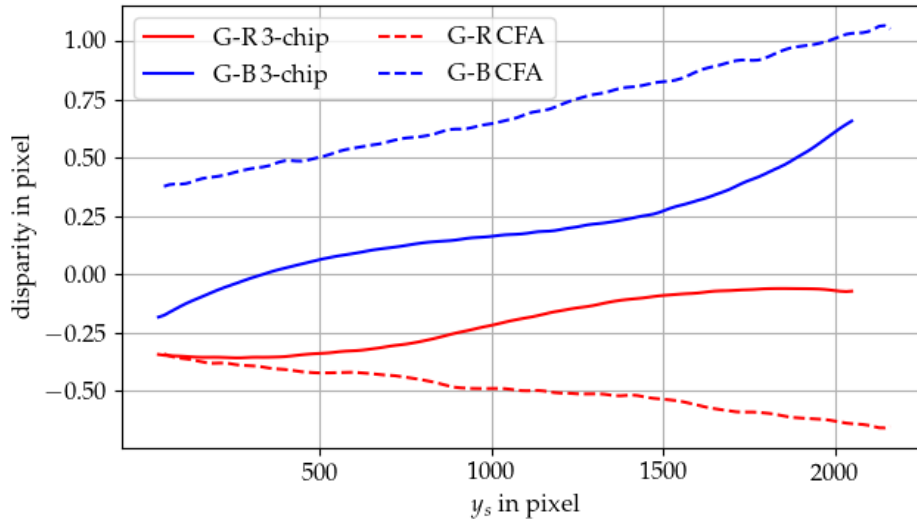


Figure 11. Profil plot that shows the disparity component in y_s direction, averaged along x_s , and plotted over y_s . The plot shows the profile for the disparity maps G-R (red) and G-B (blue) and the CFA camera (dashed line) and the three-chip camera (solid line).

This can be explained by the superposition of the disparities due to sensor misalignment, differences in the magnification and the chromatic dispersion. The contrary sign of the G-R and G-B disparity maps results from the fact that the green color is at the center of the spectrum and the red and blue colors at the opposing edges of the spectrum.

The disparity maps, however, can not only be used to analyze the effect of the chromatic dispersion

but furthermore to correct the misalignment of the color channels by using the obtained disparity map as input to shift the red and blue color channels towards the green color channel. The principle is similar to the approach of window deformation that is commonly used during the multipass PIV processing.

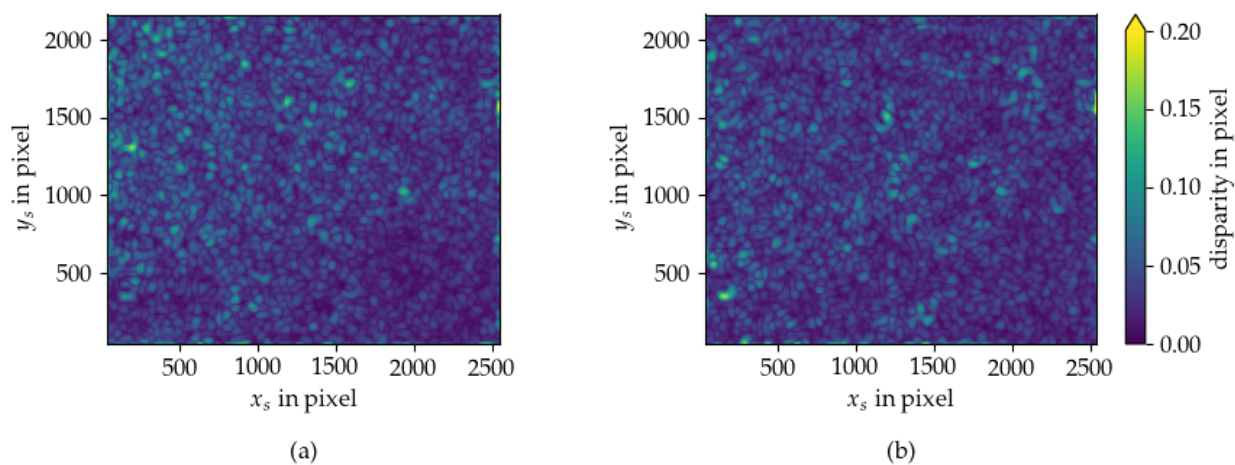


Figure 12. Disparity maps G-R (a) and G-B (b) of the three-chip camera after shifting the red and blue color channels by the initial disparity maps. The initial disparity maps were obtained by cross correlating the color channels of only a single image.

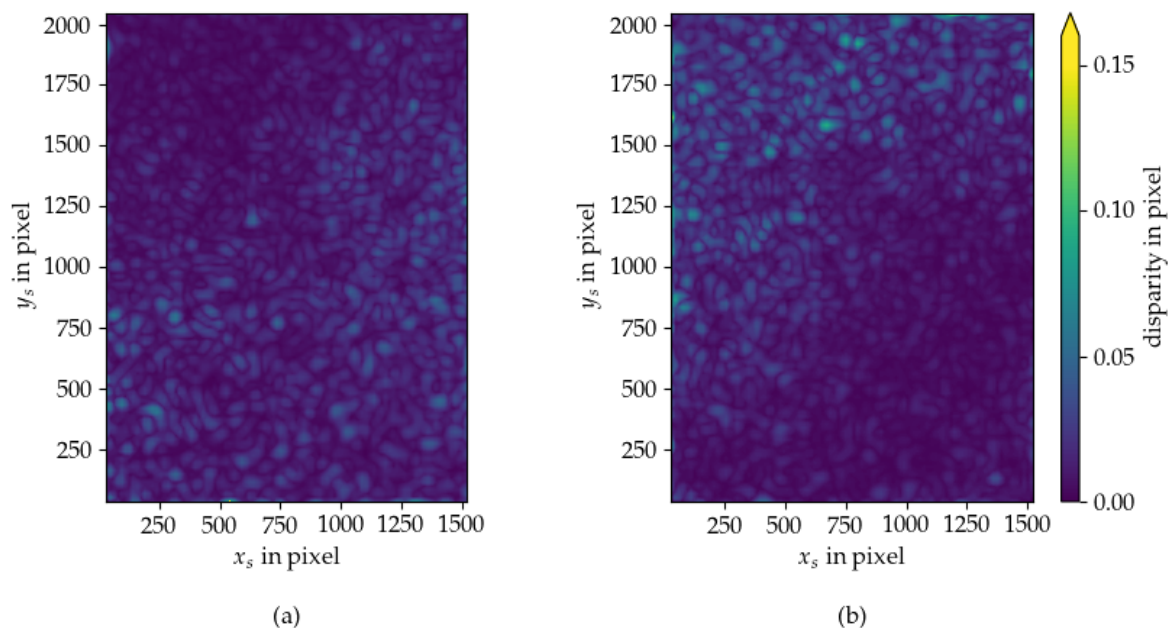


Figure 13. Disparity maps G-R (a) and G-B (b) of the CFA camera after shifting the red and blue color channels by the initial disparity maps. The initial disparity maps were obtained by cross correlating the color channels of only a single image.

The effect of shifting the red and blue color channels towards the green channel is shown in Figure 7 and Figure 8 by comparing the original images on the left with the corrected image on the right, one can distinguish a more homogeneous color distribution across the particle image and a reduction of the chromatic dispersion. To analyze the efficiency beyond a visual inspection, the disparity maps G-R and G-B were calculated again after applying the color correction. The results for the CFA camera are shown in Figure 12 and for the three-chip camera are shown in Figure 13. The remaining disparity is small, with mean disparities for the CFA camera of $0.030 \text{ pixel} \pm 0.020 \text{ pixel}$ (mean \pm standard deviation) for G-R and of $0.038 \text{ pixel} \pm 0.019 \text{ pixel}$ for G-B and for the three-chip camera of $0.011 \text{ pixel} \pm 0.008 \text{ pixel}$ (G-R) and of $0.012 \text{ pixel} \pm 0.011 \text{ pixel}$ (G-B). However, further investigation with respect to the color extraction from the corrected particle images is required for a conclusive statement.

5. Conclusion

We proposed a new approach to combine volumetric velocity measurement using Shake-the-Box with 3D Particle Image Thermometry measurements in large aspect ratio Rayleigh-Bénard convection. We successfully demonstrated that we are able to measure the 3D velocity of a convection flow in a domain that covers approximately $160 \text{ mm} \times 160 \text{ mm}$ and almost the complete cell height of 28 mm . Furthermore, we discussed the challenges that arise from color imaging of small particles and oblique viewing angles as they are common for volumetric velocity measurements and TLC-based temperature measurements. Firstly, we discussed the effect of the sparse color sampling of a CFA camera that can result in erroneous color values in cases where the particle image is close to the pixel size. We suggested a three-chip camera with a color-separating trichroic prism that samples each color at full sensor resolution as a possible solution and investigated the disparity arising from a mechanical misalignment of the sensors. Secondly, we demonstrated the influence of the chromatic dispersion due to the oblique viewing angle of the cameras. We quantified the chromatic dispersion by correlating the green and red color channels and the green and blue color channels. This analysis showed that the chromatic dispersion is largely affected by the viewing angle θ . Finally, we applied a correction step by using disparity maps to shift the red and blue color channels to align with the green color channel. We evaluated the correction method by visual comparison of the uncorrected and the corrected images and by computing the disparities between the green and red and between the green and blue color channels after applying the correction step. Both indicate significantly reduced color dispersion. This shows that the correction step is a promising approach, but further investigation with respect to a reliable color extraction is required.

Acknowledgements

The authors gratefully acknowledge the support of Dr. Thomas Fuchs from the Universität der Bundeswehr München and LaVision GmbH with the projection of the 3D position into the color camera images. Furthermore, we are very thankful for the funding through the DFG PP 1881 "Turbulente Superstrukturen" and the "DeepTurb" project of the Carl Zeiss Foundation.

References

- Anders, S., Noto, D., Tasaka, Y., & Eckert, S. (2020). Simultaneous optical measurement of temperature and velocity fields in solidifying liquids. *Experiments in Fluids*, 61(4), 1–19.
- Castaing, B., Gunaratne, G., Heslot, F., Kadanoff, L., Libchaber, A., Thomae, S., ... Zanetti, G. (1989). Scaling of hard thermal turbulence in Rayleigh-Bénard convection. *Journal of Fluid Mechanics*, 204, 1–30.
- Chillà, F., & Schumacher, J. (2012). New perspectives in turbulent Rayleigh-Bénard convection. *The European Physical Journal E*, 35(7), 58.
- Cierpka, C., Kaestner, C., Resagk, C., & Schumacher, J. (2019). On the challenges for reliable measurements of convection in large aspect ratio Rayleigh-Bénard cells in air and sulfurhexafluoride. *Experimental Thermal and Fluid Science*, 109, 109841.
- Fuchs, T., Hain, R., & Kähler, C. J. (2016). Double-frame 3D-PTV using a tomographic predictor. *Experiments in Fluids*, 57(11), 1–5.
- Gunturk, B. K., Glotzbach, J., Altunbasak, Y., Schafer, R. W., & Mersereau, R. M. (2005). Demosaicking: color filter array interpolation. *IEEE Signal Processing Magazine*, 22(1), 44–54.
- Hijazi, A., Friedl, A., Cierpka, C., Kähler, C., & Madhavan, V. (2017). High-speed imaging using 3CCD camera and multi-color LED flashes. *Measurement Science and Technology*, 28(11), 115401.
- Moller, S., König, J., Resagk, C., & Cierpka, C. (2019). Influence of the illumination spectrum and observation angle on temperature measurements using thermochromic liquid crystals. *Measurement Science and Technology*, 30(8), 084006.
- Moller, S., Resagk, C., & Cierpka, C. (2020). On the application of neural networks for temperature field measurements using thermochromic liquid crystals. *Experiments in Fluids*, 61(4), 1–21.
- Moller, S., Resagk, C., & Cierpka, C. (2021). Long-time experimental investigation of turbulent superstructures in Rayleigh-Bénard convection by noninvasive simultaneous measurements of temperature and velocity fields. *Experiments in Fluids*, 62(4).

- Pandey, A., Scheel, J. D., & Schumacher, J. (2018). Turbulent superstructures in Rayleigh-Bénard convection. *Nature communications*, 9(1), 2118.
- Ratz, M., Sachs, S., König, K., Jörg, Mendez, M., & Cierpka, C. (2022). Radial Basis Function Regression of Lagrangian Three-Dimensional Particle Tracking Data. In *20th International Symposium on Applications of Laser and Imaging Techniques to Fluid Mechanics, Lisbon, Portugal*.
- Schiepel, D., Schmeling, D., & Wagner, C. (2021). Simultaneous tomographic particle image velocimetry and thermometry of turbulent Rayleigh-Bénard convection. *Measurement Science and Technology*, 32(9), 095201.
- Segura, R., Cierpka, C., Rossi, M., Joseph, S., Bunjes, H., & Kähler, C. J. (2013). Non-encapsulated thermo-liquid crystals for digital particle tracking thermography/velocimetry in microfluidics. *Microfluidics and Nanofluidics*, 14(3-4), 445–456.
- Segura, R., Rossi, M., Cierpka, C., & Kähler, C. J. (2015). Simultaneous three-dimensional temperature and velocity field measurements using astigmatic imaging of non-encapsulated thermo-liquid crystal (TLC) particles. *Lab on a Chip*, 15(3), 660–663.